Eur. Phys. J. D **65**, 189–198 (2011)
DOI: 10.1140/epjd/e2011-20009-4

THE EUROPEAN PHYSICAL JOURNAL D

Regular Article

Scattering of Stark-decelerated OH radicals with rare-gas atoms

L. Scharfenberg[1], K.B. Gubbels[1,2], M. Kirste[1], G.C. Groenenboom[2], A. van der Avoird[2], G. Meijer[1], and S.Y.T. van de Meerakker[1,a]

[1] Fritz-Haber-Institut der Max-Planck-Gesellschaft, Faradayweg 4-6, 14195 Berlin, Germany
[2] Institute for Molecules and Materials, Radboud Universiteit Nijmegen, Heyendaalseweg 135, 6525 AJ Nijmegen, The Netherlands

Received 5 January 2011 / Received in final form 28 January 2011
Published online 15 April 2011 –

Abstract. We present a combined experimental and theoretical study on the rotationally inelastic scattering of OH ($X^2\Pi_{3/2}$, $J = 3/2, f$) radicals with the collision partners He, Ne, Ar, Kr, Xe, and D_2 as a function of the collision energy between ∼70 cm^{-1} and 400 cm^{-1}. The OH radicals are state selected and velocity tuned prior to the collision using a Stark decelerator, and field-free parity-resolved state-to-state inelastic relative scattering cross sections are measured in a crossed molecular beam configuration. For all OH-rare gas atom systems excellent agreement is obtained with the cross sections predicted by coupled channel scattering calculations based on accurate ab initio potential energy surfaces. This series of experiments complements recent studies on the scattering of OH radicals with Xe [J.J. Gilijamse, S. Hoekstra, S.Y.T. van de Meerakker, G.C. Groenenboom, G. Meijer, Science **313**, 1617 (2006)], Ar [L. Scharfenberg, J. Kłos, P.J. Dagdigian, M.H. Alexander, G. Meijer, S.Y.T. van de Meerakker, Phys. Chem. Chem. Phys. **12**, 10660 (2010)], He, and D_2 [M. Kirste, L. Scharfenberg, J. Kłos, F. Lique, M.H. Alexander, G. Meijer, S.Y.T. van de Meerakker, Phys. Rev. A **82**, 042717 (2010)]. A comparison of the relative scattering cross sections for this set of collision partners reveals interesting trends in the scattering behavior.

1 Introduction

The study of collisional energy transfer between simple atoms and molecules has been essential for our present understanding of the dynamics of molecular interactions, and for testing our ability to accurately calculate potential energy surfaces that govern these interactions [1]. Rotationally inelastic scattering is one of the simplest scattering processes, and has been studied with ever increasing level of detail during the last decades. Experimental studies at a full state-to-state level are nowadays possible, revealing detailed information on the potential energy surfaces and the resulting motion on these surfaces [2,3].

Rotationally inelastic scattering of free radical species such as OH or NO with atomic collision partners has been of special interest in molecular scattering experiments [4,5]. The scattering of these open-shell species in a $^2\Pi$ electronic state involves more than one Born-Oppenheimer potential surface, resulting in rich multi-surface dynamics with various quantum interference effects [6]. At a full state-to-state level, collision induced transitions between rotational, spin-orbit, and Λ-doublet levels have been studied [7–9]. Sophisticated beam production and product state detection methods have been developed to measure differential cross sections [10,11], the steric asymmetry of the collision [12], and the alignment or orientation of the collision products [13–16]. The wealth of scattering data that is available for these systems, together with the spectroscopic data of the bound states of relevant complexes [17,18], offers stringent tests for ab initio potential energy surfaces (PES's) and for quantum scattering calculations.

In recent years, new approaches to perform high-precision inelastic scattering experiments involving radical species have become possible with the development of the Stark-deceleration technique [19]. The Stark deceleration method exploits the concepts of charged-particle accelerator physics to produce molecular beams with a tunable velocity and almost perfect state purity [20]. The method was first applied to molecular scattering studies in 2006, when a Stark-decelerated beam of OH ($X^2\Pi_{3/2}, J = 3/2, f$) radicals was scattered with a conventional beam of Xe atoms [21]. By tuning the velocity of the OH radicals between 33 m/s and 700 m/s prior to the collision, the center-of-mass collision energy was varied between 60 cm^{-1} and 400 cm^{-1}. This energy range encompasses the energetic thresholds for inelastic scattering to the first excited rotational levels of the OH radical, and the threshold behavior of the inelastic state-to-state cross sections was accurately determined. Excellent agreement

[a] e-mail: basvdm@fhi-berlin.mpg.de

was found with cross sections derived from coupled channel calculations on ab initio computed potential energy surfaces.

Since this first proof-of-principle experiment, a new crossed beam scattering apparatus was developed that employs an improved version of the Stark decelerator. With this decelerator, packets of OH radicals can be produced with a superior number density, a narrower velocity spread, and a higher quantum state purity [22]. This apparatus enables state-to-state scattering experiments as a function of the collision energy with a sensitivity that exceeds that of conventional crossed beam scattering experiments. This was demonstrated first on the benchmark OH ($X^2\Pi$)-Ar system, for which parity-resolved integral state-to-state scattering cross sections for in total 13 inelastic scattering channels have been determined as a function of the collision energy [23]. Recently, the same methodology was applied to the scattering of OH radicals with He atoms and D_2 molecules [24].

These experiments challenge the most accurate potential energy surfaces and quantum scattering calculations presently available. For the scattering of OH radicals with Ar and He atoms, excellent agreement was found between experiment and theory, although at high collision energies and for specific inelastic channels deviations were found. For the OH-He system, the almost perfect quantum state purity offered by the Stark decelerator enabled the observation of the strong propensities for preferred excitation into final states of certain parity that had been predicted for this system [7].

Here we report new measurements on the rotationally inelastic scattering of OH ($X^2\Pi_{3/2}, J = 3/2, f$) radicals with Ne, Kr, and Xe atoms at collision energies between 60 cm^{-1} and 400 cm^{-1}. The measured cross sections for the OH-Xe system confirm the cross sections that were determined for this system in our earlier work [21]. For all three systems, excellent agreement is obtained with cross sections that are derived from quantum scattering calculations based on available potential energy surfaces.

These studies complement our previous investigations on the scattering of OH radicals with He atoms, Ar atoms and D_2 molecules, and together form a complete data set on the scattering of OH radicals with rare-gas atoms. A comparison of the relative scattering cross sections for the various collision partners is presented that reveals interesting trends in the scattering behavior.

2 Experiment

2.1 Experimental setup

The experiments are performed in a crossed molecular beam apparatus that is schematically shown in Figure 1. A detailed description of this machine, as well as of the production, Stark deceleration, and detection of OH radicals can be found in references [22,23]; only the most essential aspects of the experiment are described here.

A pulsed supersonic beam of OH radicals is created by photolysis of nitric acid seeded in either krypton or argon. After the supersonic expansion nearly all OH radicals reside in the lowest rotational ($J = 3/2$) and vibrational level of the $X^2\Pi_{3/2}$ electronic ground state. The two Λ-doublet components of this level, labeled e and f, are populated equally in the beam since their energy difference is only 0.05 cm^{-1}. OH radicals that reside in the energetically higher lying f-component can be focused and velocity tuned using the Stark decelerator, whereas OH radicals in the e-component are deflected from the beam axis. After passing a skimmer, the packet of OH radicals enters the 3×3 mm^2 opening of the decelerator. A sequence of high voltage pulses is applied to the decelerator electrodes to generate time-dependent electric field configurations that either decelerate, guide or accelerate the OH radicals. The Stark decelerator that is used here employs the so-called $s = 3$ operation mode [25,26], and has been described in detail in reference [22].

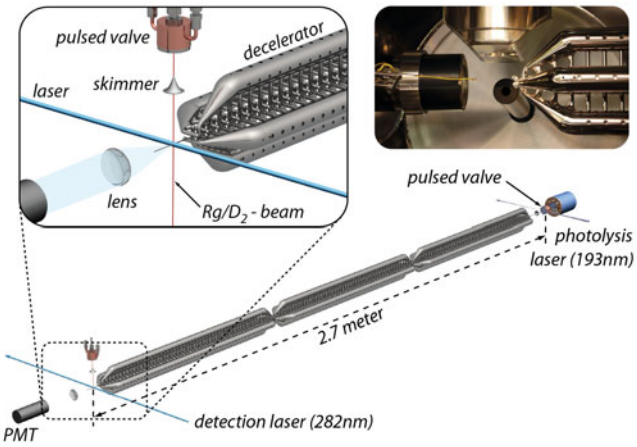

Fig. 1. (Color online) Scheme of the experimental setup. A pulsed beam of OH radicals is produced by laser photolysis of HNO_3 seeded in either Kr or Ar. The radicals pass a 2.6 m long Stark decelerator and are scattered by a pulsed beam of rare-gas (Rg) atoms or D_2 molecules. The OH radicals are state-selectively detected using a laser-induced fluorescence scheme. The fluorescence is imaged onto a photo multiplier tube by a lens. The upper right inset shows a photograph of the beam crossing region with lens holder, light baffle, and the exit of the Stark decelerator. The secondary beam source is protruding from the top.

The packet of OH ($X^2\Pi_{3/2}, J = 3/2, f$) radicals that emerges from the decelerator has a quantum state purity of >99% and intersects the central axis of the secondary beam at an angle of 90° at a distance of 16.5 mm from the decelerator exit. Collisions take place in a field free region and the initially uneven distribution over M_J-components which is present inside the decelerator is assumed to be scrambled completely while the molecules move towards the collision region.

A temperature controlled solenoid valve produces the secondary beam of rare-gas atoms or D_2 molecules. The mean forward velocity of this beam is inferred from a time-of-flight measurement using two microphone-based beam

detectors that are placed 300 mm apart. To ensure single-collision conditions, the intensity of the secondary beam is kept sufficiently low so that the decrease of the initial population in the $J = 3/2, f$ level remains below 4%.

The collision products are state-selectively detected via saturated laser-induced fluorescence when the most intense part of the OH packet is in the center of the collision region. A pulsed dye laser is used to induce various rotational transitions of the $A^2\Sigma^+, v = 1 \leftarrow X^2\Pi, v = 0$ band. The laser beam intersects both molecular beams under 90° and the off-resonant fluorescence is collected by a lens and imaged onto a photomultiplier tube (see the inset of Fig. 1).

2.2 Measurement procedure and data analysis

The collision energy range between 60 and 400 cm^{-1} is covered using two measurement intervals with overlapping energy, as described in reference [23]. For these intervals, molecular beams of OH radicals are produced using Kr and Ar as seed gases, resulting in OH radical beams with mean initial velocities of 430 m/s and 615 m/s, respectively. Within each interval, the collision energy is varied by tuning the velocity of the OH radicals prior to the collision using the Stark decelerator. For collisions with Ne, Ar, Kr and Xe atoms, the mean velocity of the rare-gas atom beam is kept constant for all measurements. The mean speed and corresponding valve temperatures for the different rare-gas beams are: 445 m/s (Ne, 93 K), 400 m/s (Ar, 110 K), 330 m/s (Kr, 163 K) and 300 m/s (Xe, 220 K). For collisions with He atoms and D_2 molecules, the small reduced mass makes it inconvenient to vary the collision energy by solely tuning the speed of the OH packet. Therefore, the speed of the secondary beam is varied in comparatively large steps by changing the temperature of the valve. For a given valve temperature, the OH velocity is then tuned from 168 to 741 m/s. The D_2 molecules are assumed to be distributed between ortho and para rotational levels according to the statistical weights, i.e., 67% of the molecules are expected to populate rotational levels with J even and 33% levels with J odd.

The Stark decelerator provides packets of OH radicals at a rate of 10 Hz. The secondary beam is operated at 5 Hz and collision signals are inferred from the fluorescence intensity difference between alternating shots of the experiment. To limit the effects of long-term drifts in the experiment, the collision energy dependence of the scattering channels is measured via a quasi-continuous cycle [23]. In such cycle, the collision energy is scanned automatically by producing a different velocity of the OH radicals for every shot of the experiment. The collision signals are obtained from typically 1000 runs of the experiment, and quoted error bars represent the statistical fluctuation of the measured mean values. Both photon counting and analog detection are used in the data acquisition [23].

Our experiment is not sensitive to elastic scattering; only scattering events that change the internal quantum state of the OH radical can be detected. Within the studied collision energy range, collisional excitation to at most 13 rotational levels can occur. These levels are labeled as $F_1(Je/f)$ and $F_2(Je/f)$, where F_1 and F_2 denote the $X^2\Pi_{3/2}$ and the $X^2\Pi_{1/2}$ spin-orbit manifolds, respectively, and the parity labels e and f correspond to the two Λ-doublet components of each rotational level. An energy level diagram with all relevant rotational levels is shown in Figure 3. Note that the Λ-doublet splitting is largely exaggerated in this figure for reasons of clarity. The rotational transitions that are used to probe the individual levels, as well as the excitation rates that are used to convert measured fluorescence intensities to populations, are specified in Table 2 of reference [23].

The experimental scattering signals are most easily compared with theoretical calculations when relative inelastic scattering cross sections are derived from the observations. The relative scattering cross section for a specific channel is proportional to the total number of molecules that is detected in the corresponding quantum state. However, the detection volume is necessarily limited and in general not all molecules can be detected. A density-to-flux transformation is required to relate the measured relative populations in final states to relative scattering cross sections. Under our experimental conditions, the resulting correction is small, as is discussed in detail in the appendix of reference [23]. For the scattering of OH with Ne, Ar, Kr and Xe atoms, we have performed the transformation using the differential cross sections determined from theory. For He and D_2, the density-to-flux correction can be safely omitted due to the small mass of the collision partner compared to the mass of the OH radical.

3 Theory

The theory for the scattering of $^2\Pi$-state molecules with ^1S-state atoms is well established [27]. In particular, collision studies between OH molecules and rare-gas atoms at low collision energies have received a lot of attention over the last years [21,28–30]. In this section we only give a brief summary of the relevant theory. A more extensive account can be found in reference [31].

The Hamiltonian that describes the scattering of ground state OH ($X^2\Pi$) with rare-gas atoms is given by

$$\hat{H} = \frac{-\hbar^2}{2\mu R}\frac{\partial^2}{\partial R^2}R + \frac{\hat{L}^2}{2\mu R^2} + \sum_{\Lambda',\Lambda} |\Lambda'\rangle V_{\Lambda',\Lambda}(R,\theta)\langle\Lambda| + \hat{H}_{\mathrm{OH}}, \tag{1}$$

where R is the length of the vector $\mathbf{R}$ that connects the center-of-mass of the OH molecule and the rare-gas atom, μ is the reduced mass of the atom-OH complex, $\hat{L}$ is the angular momentum operator corresponding to end-over-end rotation of the OH-rare gas atom complex, and $\hat{H}_{\mathrm{OH}}$ is the Hamiltonian of the OH molecule in the ($X^2\Pi$) ground state. The $X^2\Pi$ electronic ground state of the OH radical has two degenerate components with projections $\Lambda = \pm 1$ of the orbital electronic angular momentum on the internuclear $\hat{r}$-axis. The OH-rare gas interaction is represented by the operators $|\Lambda'\rangle V_{\Lambda',\Lambda}(R,\theta)\langle\Lambda|$ that couple different electronic states Λ and Λ'. The angle θ defines the

angle between the unit vector $\hat{R}$ and the OH bond direction $\hat{r}$, with $\theta = 0$ corresponding to collinear atom-HO. The Hamiltonian of OH includes rotation, spin-orbit coupling and Λ-doubling, where we use the OH rotational constant $B = 18.5487$ cm^{-1}, the spin-orbit coupling constant $A = -139.21$ cm^{-1}, and Λ-doubling parameters $p = 0.235$ cm^{-1} and $q = -0.0391$ cm^{-1} [32]. From equation (1) it follows that differences in the collisions between OH and the various rare gas atoms originate from the differences in the interaction potential and the reduced mass.

When the rare-gas atom approaches the OH molecule, the electronic degeneracy of the Π state is lifted. The resulting matrix elements $V_{\Lambda,\Lambda'}$ of the potential are nonzero for $\Lambda' - \Lambda = 0, \pm 2$, and two potential energy surfaces are involved in the scattering process. The potential energy surfaces can be expanded in Racah normalized spherical harmonics

$$V_{1,1} = V_{-1,-1} = \frac{V_{A'} + V_{A''}}{2} = \sum_l v_{l,0}(R) C_{l,0}(\theta, 0),$$
$$V_{1,-1} = V_{-1,1} = \frac{V_{A''} - V_{A'}}{2} = \sum_l v_{l,2}(R) C_{l,2}(\theta, 0), \quad (2)$$

where A' and A'' refer to the reflection symmetry of the electronic states. The surfaces $V_{1,1}$ and $V_{1,-1}$ are often referred to as the sum $V_{\rm sum}$ and difference $V_{\rm diff}$ potential energy surface, respectively.

Ab initio calculations for the OH-atom interaction energy can be performed using the MOLPRO program package [33], which has resulted in potentials for the OH-He [34], OH-Ne [34,35], OH-Ar [23], OH-Kr [36] and OH-Xe [21] complexes. The most relevant properties of the various interacting systems, such as the reduced mass of the OH-rare gas atom complex, the polarizability of the rare gas atom, the minima of the potential energy surfaces in the two different linear configurations of the complex ($\theta = 0°$ and $\theta = 180°$), as well as the position and energy of the minimum of the A' potential at a nonlinear geometry, are listed in Table 1.

The potential energy surfaces vary in the quality of the basis set used, and the quality of the method. All potentials used the counterpoise procedure to correct for the basis set superposition error [37]. The OH-He and the OH-Ne potentials of Lee et al. were both calculated with a spin-restricted coupled-cluster method with single and double excitations and perturbative triples [RCCSD(T)]. The augmented triple-zeta correlation-consistent basis set (aug-cc-pVTZ) was used with an additional (3s, 3p, 2d, 2f, 1g) set of bond functions centered in the midpoint of the vector $\mathbf{R}$ [34]. The Ne-OH potential was also calculated more recently by Sumiyoshi et al., who used an explicitly correlated, spin-unrestricted approach [UCCSD(T)-F12b] with a larger quintuple-zeta basis set (aug-cc-pV5Z) [35]. Although we calculated the cross sections for both Ne-OH potentials, we only show the results with the most recent potential, which gave a clearly better agreement with experiment. This is probably due to the larger basis set and the improved calculation method, which includes explicit electron correlations that particularly enhance the accuracy of the short-ranged behavior of the potential. For the Xe-OH potential, RCCSD(T) was used with a quadruple-zeta basis set (aug-cc-pVQZ) and with a set of (3s, 3p, 2d, 1f, 1g) mid-bond orbitals with geometry-dependent exponents [21]. For the Kr-OH potential, the UCCSD(T)-F12b approach was used with the aug-cc-pVQZ basis set [36]. Finally, the Ar-OH potential surface was calculated with a spin-unrestricted approach [UCCSD(T)], where the basis set was extrapolated to the complete basis set limit, and where also an averaging over the $v = 0$ motion of the OH molecule was performed [23]. For the other systems, the OH molecular geometry was assumed frozen at its equilibrium bond length (OH-He, Ne, Kr) or at its vibrationally averaged distance (OH-Xe).

Table 1. Properties of the Rg-OH interaction. Values for the potential minima adapted from [21,23,34–36]. Reduced mass μ in u, polarizability α in 10^{-24} cm^3, potential energy E in cm^{-1}, coordinate R in a_0, coordinate θ in degree.

Atom	μ	α	E	R	θ	PES
He	3.24	0.21	–27.1	6.54	0	A', A''
			–21.8	6.09	180	A', A''
			–30.0	5.69	68.6	A'
Ne	9.22	0.40	–59.34	6.53	0	A', A''
			–45.18	6.14	180	A', A''
			–59.60	5.82	67.6	A'
Ar	11.9	1.64	–141.7	7.01	0	A', A''
			–92.4	6.70	180	A', A''
			–137.1	6.18	74.8	A'
Kr	14.14	2.48	–172.5	7.2	0	A', A''
			–110.3	6.8	180	A', A''
			–177.0	6.25	78	A'
Xe	15.05	4.04	–202.3	7.6	0	A', A''
			–117.9	7.3	180	A', A''
			–224.4	6.45	84	A'

In order to calculate the OH monomer eigenfunctions it is convenient to use a parity adapted Hund's case (a) basis set, labeled by $|\Omega, J, M_J, p\rangle$ with J the total angular momentum of the OH molecule, Ω and M_J the projections on the molecular and space-fixed quantization axes, and p the parity under inversion. For the exact OH eigenfunctions, $|\Omega|$ is nearly a good quantum number. The total angular momentum of the OH-atom complex is represented by the operator $\hat{\boldsymbol{\mathcal{J}}} = \hat{\mathbf{J}} + \hat{\mathbf{L}}$, whose eigenfunctions are obtained by coupling the monomer basis with the spherical harmonics $|L, M_L\rangle = Y_{L,M_L}(\vartheta, \varphi)$, where ϑ and φ are the space-fixed spherical coordinates of the vector $\mathbf{R}$. Assuming that the OH bond length is fixed, we write the scattering wave functions as products of radial and angular functions,

$$\Psi^{\mathcal{J},M_\mathcal{J},\mathcal{P}}_{\beta,L} = \frac{1}{R} \sum_{\beta',L'} \chi^{\mathcal{J},M_\mathcal{J},\mathcal{P}}_{\beta',L'\leftarrow\beta,L}(R) \psi^{\mathcal{J},M_\mathcal{J},\mathcal{P}}_{\beta',L'}(\hat{R}, \hat{r}), \quad (3)$$

where β is a shorthand notation for the monomer quantum numbers (F_i, J) with i to distinguish between the F_1

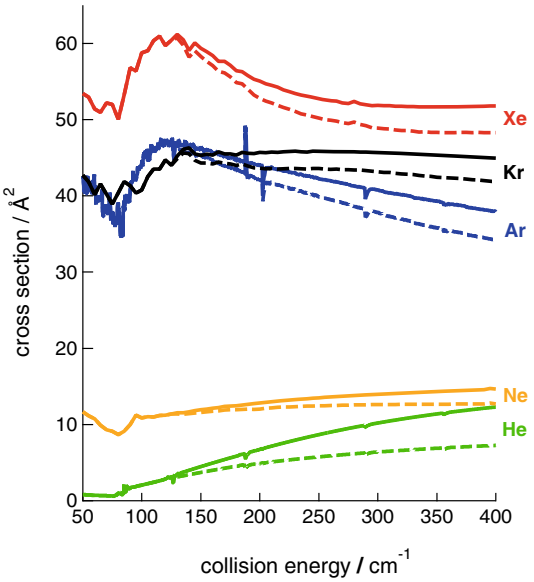

Fig. 2. (Color online) The calculated total integral cross sections for inelastic scattering of OH ($X^2\Pi_{3/2}, J = 3/2, f$) radicals with He, Ne, Ar, Kr and Xe atoms (solid lines). The contribution of transitions into the F_1 spin-orbit manifold are shown by the dashed lines.

and F_2 spin-orbit manifolds of the OH eigenstates. Note that the total angular momentum $\mathcal{J}$, its space-fixed projection $M_\mathcal{J}$ and the parity of the complex $\mathcal{P} = p(-1)^L$ are conserved in the collision process. The experimentally relevant scattering properties, i.e. the cross sections, are conveniently expressed in terms of scattering matrices, which can be obtained using standard asymptotic matching procedures [38]. The obtained S-matrices are then related to the scattering amplitudes, which in turn determine the differential cross sections [39].

In order to achieve convergence of the calculated cross-sections, we used a basis set that included all OH rotational states up to an angular momentum of $J = 21/2$, and took into account all partial wave contributions up to a total angular momentum of $\mathcal{J} = 241/2$. For the propagation of the wavefunction, the renormalized Numerov method was used, starting at $4a_0$ and continuing to $35a_0$ with a_0 the Bohr radius. The cross sections were evaluated on an energy grid with a 5 cm^{-1} interval spacing, well below the experimental energy resolution in all cases. It is noted that this energy grid is too sparse, however, to identify individual scattering resonances that occur at collision energies around the energetic thresholds.

In Figure 2, the total integral inelastic cross sections (the sum of the integral cross sections over all inelastic channels) are shown for collisions of OH ($X^2\Pi_{3/2}, J = 3/2, f$) radicals with the five different rare-gas atoms. In this figure, the contribution to the total cross section of collisions that populate levels within the F_1 manifold are indicated. The total inelastic cross section is seen to rise with increasing reduced mass, increasing atom polarizability and increasing well depth of the potential. The total inelastic cross sections as presented in Figure 2 can be used to deduce absolute state-to-state inelastic cross sections from the experimentally determined relative state-to-state cross sections. These are presented in the next section.

4 Results and discussion

4.1 Scattering of OH radicals with Ne, Kr, and Xe atoms

In this section, we first describe our new results on the scattering of OH radicals with Ne, Kr, and Xe atoms. A detailed comparison of the scattering behavior for the various systems is given in Section 4.2.

The measured relative state-to-state cross sections for the scattering of OH radicals with Ne, Kr, and Xe are shown in Figures 3 and 4. The theoretically computed cross sections, convoluted with the experimental energy resolution, are included as solid curves. For completeness, the experimental and theoretical cross sections from our previous work for the OH-He, OH-D_2, and OH-Ar systems [23,24] are also shown in these figures. The spin-orbit manifold conserving (transitions within the F_1 spin-orbit manifold) and spin-orbit manifold changing collisions (transitions from the F_1 into the F_2 manifold) are summarized in Figures 3 and 4, respectively. In both figures, the state resolved scattering channels are labeled following the color codes as indicated in the rotational energy level diagrams.

For the scattering of OH($F_1(3/2f)$) with Ne, the Λ-doublet changing $F_1(3/2f) \rightarrow F_1(3/2e)$ channel dominates at low collision energies; at energies above $\sim$150 cm^{-1} the scattering is dominated by rotational excitation to the $F_1(5/2e)$ state. For spin-orbit manifold conserving transitions, there is a strong propensity for final states of e parity. For spin-orbit manifold changing collisions, a strong Λ-doublet propensity is only observed for excitation into the $F_2(1/2)$ states. Note the little bump that is measured in the cross section for scattering into the $F_1(5/2f)$ channel at a collision energy just below 200 cm^{-1}. This bump is also measured for the OH-He system, and possibly results from scattering resonances associated with the opening of the $F_1(7/2)$ channels at a collision energy of 200 cm^{-1}. Pronounced scattering resonances are indeed predicted from the theoretical calculations for OH-He and OH-Ne at these collision energies, although their specific structure is smeared out in the experiment due to the collision energy spread.

The scattering behavior of OH with Kr is observed to be very similar to the scattering of OH with Xe atoms, and dominated by the Λ-doublet changing $F_1(3/2f) \rightarrow F_1(3/2e)$ channel at all probed collision energies. For rotational excitation, the cross sections generally rise sharply from the energetic threshold, reach a maximum, and become rather insensitive to a variation of the collision energy at higher energies. For spin-orbit manifold conserving collisions, there is a small propensity for excitation into final states of e parity. For spin-orbit changing collisions,

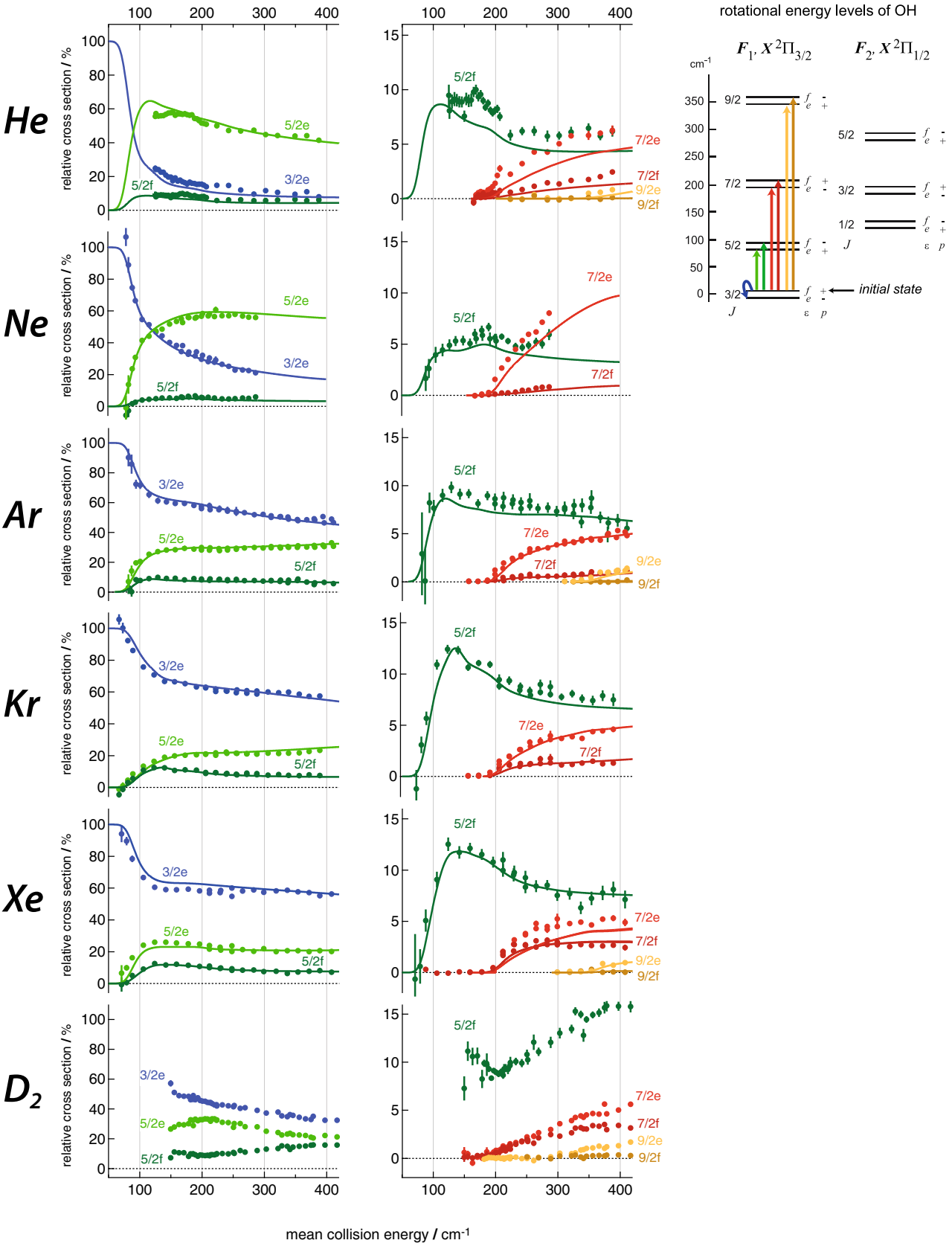

Fig. 3. (Color online) Relative state-to-state inelastic scattering cross sections for spin-orbit conserving ($F_1 \rightarrow F_1$) collisions of OH ($X^2\Pi_{3/2}, J = 3/2, f$) radicals with He, Ne, Ar, Kr, and Xe atoms and D_2 molecules as a function of the collision energy. The theoretically calculated cross sections are included as solid curves. In the energy-level scheme, the splitting between both parity components of each rotational level is greatly exaggerated for reasons of clarity.

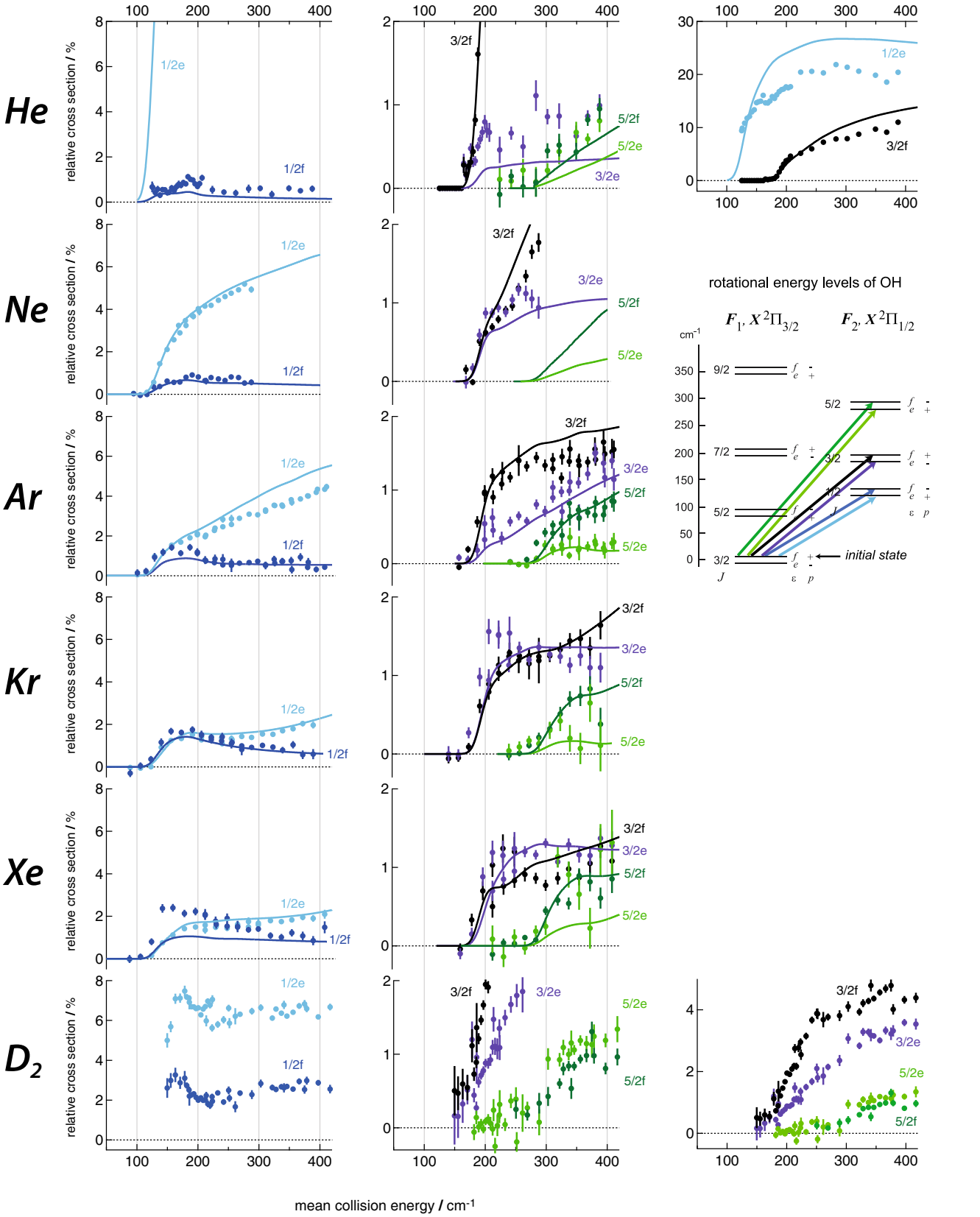

Fig. 4. (Color online) Relative state-to-state inelastic scattering cross sections for spin-orbit changing ($F_1 \rightarrow F_2$) collisions of OH ($X^2\Pi_{3/2}, J = 3/2, f$) radicals with He, Ne, Ar, Kr, and Xe atoms and D_2 molecules as a function of the collision energy. The theoretically calculated cross sections are included as solid curves.

no clear preference for excitation into one of the Λ-doublet components of a final rotational state is observed.

For all three scattering systems, the measured cross sections are compared to the cross sections determined by quantum coupled channel calculations based on high quality ab initio PES's. For the scattering of OH with Ne and Kr atoms, excellent agreement is found between the experimentally determined and theoretically computed scattering cross sections. The cross sections for all scattering channels, both for spin-orbit conserving and spin-orbit changing collisions, and for all collision energies are perfectly reproduced by the calculations.

For the scattering of OH radicals with Xe atoms, the measured cross sections confirm the cross sections that were determined in our previous work on this system [21]. It is noted that both experiments were performed in different apparatuses and with different levels of sensitivity. For the present experiment, in which state-to-state cross sections for a larger number of final states are measured, excellent agreement is obtained between experimental and theoretical cross sections. The relative scattering cross sections, as well as the threshold behavior of individual channels, are reproduced well. Also the increase in the relative scattering cross section for the $F_1(3/2f) \rightarrow F_1(5/2e)$ channel at collision energies just above the energetic threshold is perfectly reproduced. The only pronounced difference between experiment and theory is observed for the $F_2(1/2f)$ channel at energies just above threshold. This discrepancy could possibly be explained by small imperfections in the difference potential. We have observed in the calculations that the cross sections for scattering into the $F_2(1/2)$ channels are particularly sensitive to small variations of $V_{\rm diff}$. At low collision energies, there appears to be a small shift of a few $\rm cm^{-1}$ between the experimental and the theoretical values for the collision energy. The origin of this shift is not known, but could well be the result of an uncertainty in our Xe beam velocity measurements.

4.2 Comparison between the various collision partners

Interesting trends are observed when the general scattering behavior for the various OH-rare gas atom systems are qualitatively compared with each other. For the series OH-He, Ne, Ar, Kr, Xe it is observed that the role of the $F_1(3/2f) \rightarrow F_1(3/2e)$ channel gradually increases. At the same time, propensities for preferred scattering into the e parity state of the other rotational states of the F_1 manifold tend to get weaker. Finally, the contribution of the spin-orbit changing $F_1(3/2f) \rightarrow F_2(1/2e)$ channel to the scattering is gradually reduced from ~20% for OH-He to ~2% for OH-Xe. We note that these qualitative changes are strongest when the collision partner He is replaced by Ne, and when Ne is replaced by Ar. When Ar is replaced by Kr, smaller changes are observed, while hardly any changes occur in going from Kr to Xe. The scattering of OH radicals with D_2 molecules does not fit entirely in this trend; the overall scattering behavior for this system resembles that of the OH-Ar, OH-Kr and OH-Xe systems.

A qualitative understanding of the inelastic scattering of OH radicals with rare-gas atoms can be obtained from a general analysis given by Dagdigian et al. [40]. According to this analysis, the relative strength of the various scattering channels (in particular for low values of J) can be estimated from the rotational energy level structure of the OH radical and the different expansion coefficients $v_{l,0}(R)$ and $v_{l,2}(R)$ of the sum and difference potential energy surfaces, respectively.

A close inspection of the nature of the interaction potential and the relevant coefficients that determine the state-to-state cross sections can yield a satisfying understanding of the physical origin of general scattering features [41]. As outlined in reference [24], for instance, the profound difference in the scattering behavior that is observed for the inelastic scattering of OH with He atoms or D_2 molecules can be explained by the much larger anisotropy of the OH-D_2 PES's compared to the OH-He PES's. In general, a small $F_1(3/2f) \rightarrow F_1(3/2e)$ Λ-doublet changing cross section, a strong propensity for rotational excitation into the e parity component of the $F_1(5/2)$ state, and a strong cross section for scattering into the $F_2(1/2e)$ level indicates that the scattering is dominated by the symmetric l = even terms, whereas the opposite scattering behavior is expected for systems in which the asymmetric l = odd terms play a large role. The former is the case for the weakly interacting OH-He system that results in a potential energy surface with small anisotropy; the latter applies to the strongly interacting OH-D_2 system.

These qualitative arguments can also be used to rationalize the trends that are observed for the scattering of OH with the series of rare-gas atoms He, Ne, Ar, Kr, and Xe. Indeed, with increasing polarizability of the collision partner, the scattering is governed by potential energy surfaces with increasing well depth and larger anisotropy. This results in more dominant l = odd expansion coefficients, and hence in a larger $F_1(3/2f) \rightarrow F_1(3/2e)$ Λ-doublet cross section, smaller e over f propensities for excitation into the $F_1(5/2)$ state, and reduced cross sections for the $F_1(3/2f) \rightarrow F_2(1/2e)$ spin-orbit changing channel.

The trends that are observed are thus consistent with what may be expected from the nature of the OH-rare gas atom interaction potential. However, for the series of collision partners also dynamic effects that are related to the increasing mass of the collision partner may play a role. It is not a priori clear which features in the scattering behavior are due to the effect of the PES, and which features result from the effect of the reduced mass.

To study the influence of both parameters on the scattering, we have performed calculations for two hypothetical OH-rare gas atom systems. In the first system, we have used the OH-He PES's, but performed the scattering calculations with the He atom mass replaced by the Xe atom mass. In the second system, we have used the OH-Xe PES's, but performed the scattering calculations with the Xe atom mass replaced by the He atom mass. These model systems thus yield information on the

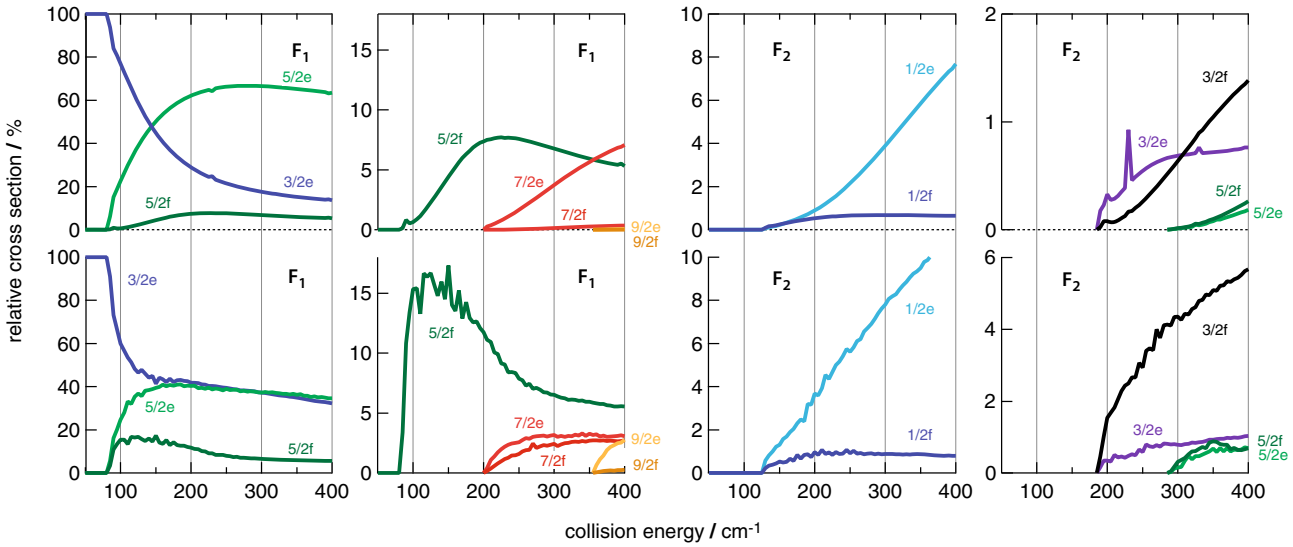

Fig. 5. (Color online) Calculated relative state-to-state inelastic scattering cross sections for two hypothetical OH ($X^2\Pi_{3/2}, J = 3/2, f$)-rare gas atom systems. Top row: calculations are based on the OH-He PES's from reference [34], but the scattering calculations are performed with the He atom mass replaced by the Xe atom mass. Bottom row: calculations are based on the OH-Xe PES's from reference [21], but the scattering calculations are performed with the Xe atom mass replaced by the He atom mass.

scattering of OH radicals with a weakly interacting but heavy collision partner, and with a strongly interacting but light collision partner. The resulting inelastic scattering cross sections for both systems are shown in Figure 5.

For the OH-He interaction potential, significant changes in the cross sections are observed upon replacement of the He atom mass with the Xe atom mass. In particular, the relative cross section for scattering into the $F_1(3/2e)$ state increases, while the contributions of the $F_1(5/2e)$ and $F_2(1/2e)$ channels to the scattering decrease. Note that also the threshold behavior of various channels changes significantly; the cross sections rise less sharply at collision energies above threshold. The resulting state-to-state relative inelastic cross sections closely resemble those for the OH-Ne system, i.e., of a weakly interacting system with a larger reduced mass compared to OH-He.

For the OH-Xe interaction potential, opposite changes in the scattering cross sections are observed upon replacement of the Xe mass with the He atom mass. The $F_1(3/2f) \rightarrow F_1(3/2e)$ channel becomes less dominant, and the $F_1(5/2e)$ and $F_2(1/2e)$ channels gain importance. The resulting relative state-to-state cross sections resemble those that are measured for the OH-D_2 system, i.e., of a strongly interacting system with a smaller reduced mass compared to OH-Xe.

These model calculations indicate that the nature of the potential energy surface and the reduced mass of the system can both have a profound and qualitatively similar influence on the scattering cross sections. This suggests that the interesting trends that are observed for the scattering of OH with He, Ne, Ar, Kr, and Xe are in part due to the increasing interaction strength of the OH radical with the collision partner, and in part due to the increasing mass of the rare-gas atom. It is not straightforward to disentangle the influence of both effects using ab initio potential energy surfaces and coupled channel scattering calculations as employed here. The individual influence on the scattering of properties such as well depth, anisotropy and reduced mass can be studied best using models for the potential and the scattering dynamics that allow for an independent variation of the relevant parameters [42,43].

5 Conclusions

We have presented new measurements on the state-to-state rotational inelastic scattering of Stark-decelerated OH ($X^2\Pi_{3/2}, J = 3/2, f$) radicals with Ne, Kr, and Xe atoms. For each collision system, a total of 13 inelastic scattering channels is studied at collision energies in the 70−400 cm^{-1} range. The collision energy dependence of the relative inelastic scattering cross sections, the threshold behavior of inelastic channels, and the energy dependence of the state-resolved propensities are accurately determined. Excellent agreement is found with the inelastic scattering cross sections determined from quantum coupled channel scattering calculations based on ab initio potential energy surfaces.

These measurements complement our recent studies on the scattering of the OH radicals with He atoms, Ar atoms, and D_2 molecules, and confirm the measured cross sections of our original work on the scattering of OH radicals with Xe atoms. Together, these studies represent the most complete combined experimental and theoretical study of the inelastic scattering of an open shell radical in a $^2\Pi$ electronic state with rare-gas atoms. The excellent agreement that is obtained with the cross sections that are derived from ab initio potential energy surfaces for all OH-rare

gas atom systems clearly indicates that the scattering of these systems is well understood.

Significant differences are found in the scattering behavior of OH radicals with the various collision partners, and interesting trends are observed in the relative inelastic scattering cross sections for the series OH-He, Ne, Ar, Kr, and Xe. Replacement of the He atom by heavier rare-gas atoms results in a more dominant $F_1(3/2f) \rightarrow F_1(3/2e)$ Λ-doublet changing cross section, smaller propensities for preferred excitation into one of the Λ-doublet components of excited rotational levels, and reduced cross sections for the $F_1(3/2f) \rightarrow F_2(1/2e)$ transition. These trends result in part from the increasing strength of the OH-rare gas atom interaction, and in part from the increasing mass of the rare-gas atom.

The resonances in the scattering of OH with He and Ne atoms at energies close to threshold – hinted at in the present measurements – will be subject of future experiments with increased collision energy resolution [44].

This work is supported by the ESF EuroQUAM programme, and is part of the CoPoMol (Collisions of Cold Polar Molecules) project. The expert technical assistance of G. Hammer, H. Haak, U. Hoppe and the FHI mechanical and electronics workshops are gratefully acknowledged. We thank A. McCoy and Y. Sumiyoshi for providing us the required information to evaluate the fit to the OH-Ne and OH-Kr potentials, and thank L. Janssen and J. Kłos for help and discussions. A.v.d.A. thanks the A. von Humboldt Foundation for a Research Award.

References

1. R.D. Levine, R.B. Bernstein, *Molecular reaction dynamics and chemical reactivity* (Oxford University Press, New York, 1987)
2. A. Schiffman, D.W. Chandler, Int. Rev. Phys. Chem. **14**, 371 (1995)
3. K. Liu, R.G. MacDonald, A.F. Wagner, Int. Rev. Phys. Chem. **9**, 187 (1990)
4. D.W. Chandler, S. Stolte, Gas Phase Molecular Reaction and Photodissociation Dynamics, in *Inelastic energy transfer: the NO-rare gas system* (Transworld Research Network, 2007), pp. 1–63
5. J.C. Whitehead, Rep. Prog. Phys. **59**, 993 (1996)
6. H. Kohguchi, T. Suzuki, Ann. Rep. Prog. Chem. Sect. C **98**, 421 (2002)
7. K. Schreel, J. Schleipen, A. Eppink, J.J. ter Meulen, J. Chem. Phys. **99**, 8713 (1993)
8. M.C. van Beek, J.J. ter Meulen, M.H. Alexander, J. Chem. Phys. **113**, 628 (2000)
9. J.J. van Leuken, F.H.W. van Amerom, J. Bulthuis, J.G. Snijders, S. Stolte, J. Phys. Chem. **99**, 15573 (1995)
10. H. Kohguchi, T. Suzuki, M.H. Alexander, Science **294**, 832 (2001)
11. A. Gijsbertsen, H. Linnartz, G. Rus, A.E. Wiskerke, S. Stolte, D.W. Chandler, J. Kłos, J. Chem. Phys. **123**, 224305 (2005)
12. S. Stolte, Nature **353**, 391 (1991)
13. M.C. van Beek, G. Berden, H.L. Bethlem, J.J. ter Meulen, Phys. Rev. Lett. **86**, 4001 (2001)
14. G. Paterson, S. Marinakis, M.L. Costen, K.G. McKendrick, J. Kłos, R. Toboła, J. Chem. Phys. **129**, 074304 (2008)
15. G. Paterson, S. Marinakis, M.L. Costen, K.G. McKendrick, J. Kłos, R. Toboła, J. Chem. Phys., Erratum **131**, 159901 (2009)
16. G. Paterson, S. Marinakis, J. Kłos, M.L. Costen, K.G. McKendrick, Phys. Chem. Chem. Phys. **11**, 8804 (2009)
17. M.C. Heaven, Ann. Rev. Phys. Chem. **43**, 283 (1992)
18. M.C. Heaven, Int. Rev. Phys. Chem. **24**, 375 (2005)
19. S.Y.T. van de Meerakker, H.L. Bethlem, G. Meijer, Nature Physics **4**, 595 (2008)
20. H.L. Bethlem, G. Berden, G. Meijer, Phys. Rev. Lett. **83**, 1558 (1999)
21. J.J. Gilijamse, S. Hoekstra, S.Y.T. van de Meerakker, G.C. Groenenboom, G. Meijer, Science **313**, 1617 (2006)
22. L. Scharfenberg, H. Haak, G. Meijer, S.Y.T. van de Meerakker, Phys. Rev. A **79**, 023410 (2009)
23. L. Scharfenberg, J. Kłos, P.J. Dagdigian, M.H. Alexander, G. Meijer, S.Y.T. van de Meerakker, Phys. Chem. Chem. Phys. **12**, 10660 (2010)
24. M. Kirste, L. Scharfenberg, J. Kłos, F. Lique, M.H. Alexander, G. Meijer, S.Y.T. van de Meerakker, Phys. Rev. A **82**, 042717 (2010)
25. S.Y.T. van de Meerakker, N. Vanhaecke, H.L. Bethlem, G. Meijer, Phys. Rev. A **71**, 053409 (2005)
26. S.Y.T. van de Meerakker, N. Vanhaecke, H.L. Bethlem, G. Meijer, Phys. Rev. A **73**, 023401 (2006)
27. M.H. Alexander, J. Chem. Phys. **76**, 5974 (1982)
28. M. Lara, J.L. Bohn, D. Potter, P. Soldán, J.M. Hutson, Phys. Rev. Lett. **97**, 183201 (2006)
29. L. González-Sánchez, E. Bodo, F.A. Gianturco, Phys. Rev. A **73**, 022703 (2006)
30. Z. Pavlovic, T.V. Tscherbul, H.R. Sadeghpour, G.C. Groenenboom, A. Dalgarno, J. Phys. Chem. A **113**, 14670 (2009)
31. T.V. Tscherbul, G.C. Groenenboom, R.V. Krems, A. Dalgarno, Faraday Discuss. **142**, 127 (2010)
32. J.P. Maillard, J. Chauville, A.W. Mantz, J. Mol. Spectrosc. **63**, 120 (1976)
33. H.-J. Werner et al., *MOLPRO, version 2008.1, a package of ab initio programs*, see http://www.molpro.net
34. H.S. Lee, A.B. McCoy, R.R. Toczyłowski, S.M. Cybulski, J. Chem. Phys. **113**, 5736 (2000)
35. Y. Sumiyoshi, I. Funahara, K. Sato, Y. Ohshima, Y. Endo, Phys. Chem. Chem. Phys. **12**, 8340 (2010)
36. Y. Sumiyoshi, I. Funahara, K. Sato, Y. Ohshima, Y. Endo, Mol. Phys. **108**, 2207 (2010)
37. S.F. Boys, F. Bernardi, Mol. Phys. **19**, 553 (1970)
38. B.R. Johnson, J. Comput. Phys. **13**, 445 (1973)
39. M.S. Child, *Molecular Collision Theory* (Academic Press, London, 1974)
40. P.J. Dagdigian, M.H. Alexander, K. Liu, J. Chem. Phys. **91**, 839 (1989)
41. A. Degli Esposti, A. Berning, H.J. Werner, J. Chem. Phys. **103**, 2067 (1995)
42. A. Gijsbertsen, H. Linnartz, C.A. Taatjes, S. Stolte, J. Am. Chem. Soc. **128**, 8777 (2006)
43. M. Lemeshko, B. Friedrich, J. Chem. Phys. **129**, 024301 (2008)
44. L. Scharfenberg, S.Y.T. van de Meerakker, G. Meijer, Phys. Chem. Chem. Phys., in press